Research Article Vol. 58, No. 32 / 10 November 2019 / Applied Optics 8829

applied optics

Non-uniformity correction of polarization response for liquid crystal modulated polarimeters

Yuxin Zhang,[1,2,3,*] Bao Zhang,[1,2] Yongfeng Hong,[1,2] Wenda Wu,[1,2,3] and Fang Xu[1,2]

[1]Changchun Institute of Optics, Fine Mechanics and Physics, Chinese Academy of Sciences, Changchun 130033, China
[2]University of Chinese Academy of Sciences, Beijing 100049, China
[3]Key Laboratory of Airborne Optical Imaging and Measurement, Chinese Academy of Sciences, Changchun 130033, China
*Corresponding author: zhangyxxx@163.com

Received 6 August 2019; revised 17 September 2019; accepted 18 September 2019; posted 9 October 2019 (Doc. ID 374753); published 8 November 2019

Liquid crystal modulated polarimeters (LCMPs) are often used to detect the full polarization information of target scenes. In this study, a non-uniformity correction method based on reference source calibration for LCMP is proposed. We analyze the error sources of the polarimeter and establish a grayscale response model with non-uniformity noises. The gain and bias correction coefficient of each pixel is calculated based on the linear response property of the detector. The polarization parameters of each detection unit of the uniform light source with the same polarization state calculated by the corrected Stokes vector are uniform. Results show that the error of the degree of linear polarization is reduced by 5.08%, and the degree of circular polarization is reduced by 19%. Therefore, the proposed method effectively improves the non-uniformity and detection accuracy of polarimeters.

https://doi.org/10.1364/AO.58.008829

1. INTRODUCTION

Polarization imaging systems can obtain not only the 2D spatial intensity distribution of target scenes but also the polarization characteristics of targets, including the degree of polarization, angle of polarization (AOP), and ellipsometry of polarization. Such polarization information can provide target features such as surface material, shape, and roughness [1]. In particular, full polarization detection systems with circular polarization information are widely used in remote sensing [1], dehazing of foggy images [2], and underwater imaging [3].

Current polarimetric detection approaches are mainly classified as division of time [4], division of amplitude [5], division of aperture [6], division of focal plane [7], and channel modulation [8]. The liquid crystal modulated polarimeter (LCMP) involved in this study is a division-of-time full polarimeter. Liquid crystal variable phase retarders (LCVRs) and ferroelectric liquid crystal (FLCs) are commonly used polarization modulators in wideband polarization imaging systems. LCVR achieves polarization modulation by changing the phase delay, while FLC achieves polarization modulation by changing the fast-axis azimuth. In general, FLC has a faster modulation speed than LCVR and has more important application value in real-time polarization imaging. However, with the innovation of liquid crystal materials and driving methods, the response time of liquid crystal phase modulators can also reach submilliseconds [9]. By liquid crystal phase modulation, polarization detection can satisfy the minimum number of repeated measurements while using the retardation when the influence of noise is minimal. In addition, the structured liquid crystal microlens array technology has the potential to be used in focal plane polarization detection systems. However, due to the limitation of fabrication technology, LCVR has not been widely used at present [10,11]. In this study, we only discuss a polarimeter using FLC for polarization modulation.

The LCMP uses two custom FLCs and a linear polarizer, which are directly installed in front of the camera's charge-coupled device (CCD). The polarimeter can quickly modulate FLCs to four different states and acquire four polarization raw frames to calculate all four Stokes vectors of each pixel in the image [12]. The advantages of a LCMP include simple structure, access to circular polarization information, lack of moving components and need for registration [13], and high detection accuracy. Although the polarimeter does not take polarization frames simultaneously, its sampling speed is much faster than that of division-of-time polarimeters with mechanical rotation of polarizers.

However, certain FLCs and polarizers have manufacturing defects [14], and the external environment (such as mechanical stress, temperature, and humidity) influences the arrangement

of FLC molecules [15]. Detectors have noise. Consequently, the spatial response of polarimeters to the same incident light is nonuniform. Errors are introduced when polarization images are reconstructed without correction. Current correction methods for polarimeters are mainly divided into three categories, namely, optical element correction, sub-region calibration, and system calibration. Eric *et al.* first presented the eigenvalue calibration method, which considers the influence of optical elements in the calibration procedure [16]. Vedeland *et al.* presented an approach to spatial calibration of full-Stokes polarization cameras for multiple wavelengths [17]. Zhang *et al.* calibrated a polarization spectrum measurement system by correcting the polarization effect of the spectrometer [18]. However, LCMP systems have a complex Mueller matrix calibration process that requires high accuracy. These methods are either insufficiently accurate or further increase the complexity of the calibration process and the amount of data.

In this paper, we present a calibration method for minimizing non-uniformity errors for a LCMP. On the basis of the linear relationship between the detector response and the incident polarized light intensity, we calculate the correction gain and bias coefficient to ensure that the spatial output response is consistent when the input is the same. Finally, the polarization parameters, namely, degree of linear polarization (DOLP), AOP, degree of circular polarization (DOCP), and ellipticity (EP) [12], are further calculated based on the corrected Stokes vectors. The performance of our method is demonstrated by three typical polarized light detection experiments. Results show that our algorithm is effective for a LCMP. This method improves the non-uniformity of the polarization spatial response and increases the accuracy of the estimation of the polarization states of incident light.

This paper is organized as follows. Section 2 describes the principle of an LCMP camera and analyzes the causes of its spatial non-uniformity. In Section 3, the mathematical model of the response with non-uniformity errors is established, and the details of the proposed correction method are introduced. Section 4 verifies the method by experiments, and the correction effect is analyzed. Finally, the conclusion is presented in Section 5.

2. PRINCIPLE OF LCMP

An LCMP uses electrically driven liquid crystal wave plates as a substitute for the mechanical rotating polarizer to detect the different polarization states of incident light while increasing the detection of circular polarization information. In this paper, the LCMP imaging camera for full-Stokes detection is regarded as an example to analyze the proposed method. The optical schematic of the LCMP is depicted in Fig. 1. It consists of a programmable FLC wave plate with a retardance close to $\lambda/2$, another programmable FLC wave plate with a retardance close to $\lambda/4$, and a linear polarizer. The scattered light from the target scene passes through the fore-optical lens and filter and then enters the LCMP. Four different polarization states are generated by modulating FLCs with a trigger signal produced by a sensor. Finally, it is received by a photodetector and converted into a gray image.

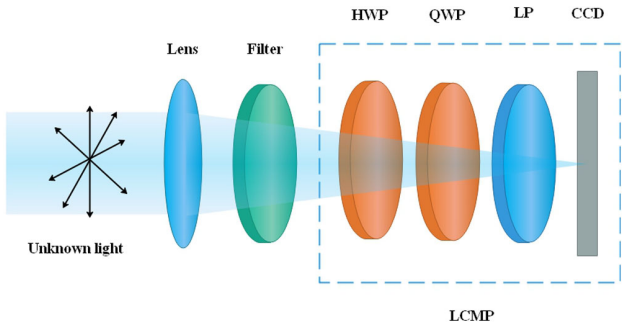

Fig. 1. Optical schematic of the LCMP. HWP, half-wave plate; QWP, quarter-wave plate; LP, linear polarizer; CCD, charge-coupled device; LCMP, liquid crystal modulated polarimeter.

The Stokes vector is usually used to describe polarized or partially polarized light [19]. It is represented by vectors S_0, S_1, S_2, and S_3, which are defined as follows in Eq. (1):

$$S=\begin{bmatrix} S_0 \\ S_1 \\ S_2 \\ S_3 \end{bmatrix}=\begin{bmatrix} \langle |E_x|^2+|E_y|^2\rangle \\ \langle |E_x|^2-|E_y|^2\rangle \\ 2\mathrm{Re}\langle E_x E_y^*\rangle \\ -2\mathrm{Im}\langle E_x E_y^*\rangle \end{bmatrix}, \tag{1}$$

where E_x and E_y represent the amplitudes of the electric field vector E in the x direction and y direction, respectively, which are orthogonal to each other in the plane perpendicular to the propagation direction of the plane light wave.

The Stokes vector of the emitted light with different polarization states after LCMP modulation can be expressed as follows:

$$S_{\mathrm{out}}^{\mathrm{state}\,k} == M_{\mathrm{lcmp}}^{\mathrm{state}\,k} S_{\mathrm{in}}. \tag{2}$$

Here $M_{\mathrm{lcmp}}^{\mathrm{state}\,k}$ is the comprehensive Mueller matrix of the LCMP system under different polarization states. It reflects the transmission characteristics of the system and can be expanded into a 4×4 real matrix as follows in Eq. (3):

$$M_{\mathrm{lcmp}}^{\mathrm{state}\,k}=\begin{bmatrix} m_{11}^{\mathrm{state}\,k} & m_{12}^{\mathrm{state}\,k} & m_{13}^{\mathrm{state}\,k} & m_{14}^{\mathrm{state}\,k} \\ m_{21}^{\mathrm{state}\,k} & m_{22}^{\mathrm{state}\,k} & m_{23}^{\mathrm{state}\,k} & m_{24}^{\mathrm{state}\,k} \\ m_{31}^{\mathrm{state}\,k} & m_{32}^{\mathrm{state}\,k} & m_{33}^{\mathrm{state}\,k} & m_{34}^{\mathrm{state}\,k} \\ m_{41}^{\mathrm{state}\,k} & m_{42}^{\mathrm{state}\,k} & m_{43}^{\mathrm{state}\,k} & m_{44}^{\mathrm{state}\,k} \end{bmatrix}. \tag{3}$$

On the basis of the definition of the Stokes vector, S_0 is proportional to the total light intensity. The total intensity of the four polarization states is related only to the first row of the Muller matrix and can be written as follows in Eq. (4):

$$\begin{bmatrix} I_{\mathrm{state}\,1} \\ I_{\mathrm{state}\,2} \\ I_{\mathrm{state}\,3} \\ I_{\mathrm{state}\,4} \end{bmatrix}\propto\begin{bmatrix} S_{0,\mathrm{out}}^{\mathrm{state}\,1} \\ S_{0,\mathrm{out}}^{\mathrm{state}\,2} \\ S_{0,\mathrm{out}}^{\mathrm{state}\,3} \\ S_{0,\mathrm{out}}^{\mathrm{state}\,4} \end{bmatrix}$$

$$=\begin{bmatrix} m_{11}^{\mathrm{state}\,1}\cdot S_{0,\mathrm{in}}+m_{12}^{\mathrm{state}\,1}\cdot S_{1,\mathrm{in}} & +m_{13}^{\mathrm{state}\,1}\cdot S_{2,\mathrm{in}}+m_{14}^{\mathrm{state}\,1}\cdot S_{3,\mathrm{in}} \\ m_{11}^{\mathrm{state}\,2}\cdot S_{0,\mathrm{in}}+m_{12}^{\mathrm{state}\,2}\cdot S_{1,\mathrm{in}} & +m_{13}^{\mathrm{state}\,2}\cdot S_{2,\mathrm{in}}+m_{14}^{\mathrm{state}\,2}\cdot S_{3,\mathrm{in}} \\ m_{11}^{\mathrm{state}\,3}\cdot S_{0,\mathrm{in}}+m_{12}^{\mathrm{state}\,3}\cdot S_{1,\mathrm{in}} & +m_{13}^{\mathrm{state}\,3}\cdot S_{2,\mathrm{in}}+m_{14}^{\mathrm{state}\,3}\cdot S_{3,\mathrm{in}} \\ m_{11}^{\mathrm{state}\,4}\cdot S_{0,\mathrm{in}}+m_{12}^{\mathrm{state}\,4}\cdot S_{1,\mathrm{in}} & +m_{13}^{\mathrm{state}\,4}\cdot S_{2,\mathrm{in}}+m_{14}^{\mathrm{state}\,4}\cdot S_{3,\mathrm{in}} \end{bmatrix}. \tag{4}$$

The determination of $m_{1j}^{\text{state }k}$ requires N ($N > 4$) sets of known incident Stokes vectors S_{in}^N and measured $S_{0,\text{out}}^N$ because of the existence of system noise. The square method is used to obtain the optimal solution. For the kth state of the LCMP, the transmission relations can be expressed in matrix form as

$$\begin{bmatrix} S_{0,\text{out}}^1 \\ S_{0,\text{out}}^2 \\ \vdots \\ S_{0,\text{out}}^N \end{bmatrix} = \begin{bmatrix} S_{0,\text{in}}^1 & S_{1,\text{in}}^1 & S_{2,\text{in}}^1 & S_{3,\text{in}}^1 \\ S_{0,\text{in}}^2 & S_{1,\text{in}}^2 & S_{2,\text{in}}^2 & S_{3,\text{in}}^2 \\ \vdots & \vdots & \vdots & \vdots \\ S_{0,\text{in}}^N & S_{1,\text{in}}^N & S_{2,\text{in}}^N & S_{3,\text{in}}^N \end{bmatrix} \cdot \begin{bmatrix} m_{11}^k \\ m_{12}^k \\ m_{13}^k \\ m_{14}^k \end{bmatrix}$$

$$= (S_{\text{in}}^N)^T \cdot \begin{bmatrix} m_{11}^k \\ m_{12}^k \\ m_{13}^k \\ m_{14}^k \end{bmatrix}. \tag{5}$$

The first row of the Mueller matrix of each polarization state of the LCMP can be solved by the Moore–Penrose pseudo-inverse A^+ as follows:

$$\begin{bmatrix} m_{11}^{\text{state }k} \\ m_{12}^{\text{state }k} \\ m_{13}^{\text{state }k} \\ m_{14}^{\text{state }k} \end{bmatrix} = [(S_{\text{in}}^N)^T]^+ \cdot \begin{bmatrix} S_{0,\text{out}}^1 \\ S_{0,\text{out}}^2 \\ \vdots \\ S_{0,\text{out}}^N \end{bmatrix}. \tag{6}$$

Here we obtain the polarization state measurement matrix X of the polarimeter as

$$X = \begin{bmatrix} m_{11}^{\text{state }1} & m_{12}^{\text{state }1} & m_{13}^{\text{state }1} & m_{14}^{\text{state }1} \\ m_{11}^{\text{state }2} & m_{12}^{\text{state }2} & m_{13}^{\text{state }2} & m_{14}^{\text{state }2} \\ m_{11}^{\text{state }3} & m_{12}^{\text{state }3} & m_{13}^{\text{state }3} & m_{14}^{\text{state }3} \\ m_{11}^{\text{state }4} & m_{12}^{\text{state }4} & m_{13}^{\text{state }4} & m_{14}^{\text{state }4} \end{bmatrix}. \tag{7}$$

The inverse of the matrix X is defined as the data reduction matrix (DRM) [20]. Finally, any unknown incident Stokes vectors can be estimated by Eq. (8) as follows:

$$\widehat{S_{\text{in}}} = X^{-1} \cdot S_{0,\text{out}}. \tag{8}$$

Under ideal conditions, $S_{0,\text{out}}$ is proportional to the intensity of the emitted light, and the incident irradiance is linearly related to the photoelectric response of the detector. Therefore, this type of polarimeter usually uses the gray information obtained by the polarization camera to calibrate the DRM directly. After calibrating the DRM matrix, the polarimeter uses the gray information collected to estimate the incident Stokes vector and further calculates the polarization information, such as DOLP and DOCP. This calculation method is based on the following assumptions.

1. The system has no fixed noise, the intensity of light is proportional to the gray level, and no bias factor exists.
2. The spatial arrangement of liquid crystal molecules in FLCs is consistent.
3. The photoelectric response of each pixel in the whole detector is consistent.

However, in practical applications, first, the spatial response of components to the same incident light is not uniform due to the local differences in the structure materials and manufacturing process of FLCs and polarizers. Second, the photoelectric response of each pixel cannot be exactly the same due to the limitation of the manufacturing level of CCD devices; moreover, fixed noise, such as dark current noise and shot noise, exists [21]. Finally, the detector will have a proportion of blind pixels when it is produced from the factory. These factors directly lead to spatial response non-uniformity of the intensity of the same incident light, which then leads to spatial response non-uniformity of the polarization information of the polarimeter. Therefore, we should develop a method of correcting and reconstructing polarization information to eliminate fixed noise, compensate for blind pixels, and correct the non-uniformity errors of the spatial response of the polarimeter to improve the accuracy of polarization information detected by polarization cameras.

3. CORRECTION METHOD

A. Derivation of the Theoretical Model

An analysis of the actual situation reveals that the Stokes vector of the output light is proportional to the intensity, and the gray value is linear with the incident irradiance, which can be expressed as Eqs. (9) and (10) as follows:

$$S_{0,\text{out}} = \alpha I, \tag{9}$$

$$\text{DN} = \beta I + \text{DN}_{\text{dark}} + \text{DN}_{\text{random}}, \tag{10}$$

where α and β are proportional coefficients, DN represents the actual image grayscale, and DN_{dark} and $\text{DN}_{\text{random}}$ denote dark current noise and random noise, respectively. It should be noted that shot noise is included in the definition of random noise because the process of signal charge generated by light injection into the photosensitive region is random, and the number of photogenerated charges produced per unit time slightly fluctuates the characteristics of random noise. In addition to shot noise, random noise includes camera-readout noise composed of multiple noise sources, which are introduced in the process of converting the number of electrons into the gray value of each pixel. Therefore, the actual Stokes vector should be expressed as

$$S_{0,\text{out}}^{\text{state }k} = \frac{\alpha}{\beta}(\text{DN}^{\text{state }k} - \text{DN}_{\text{dark}}^{\text{state }k} - \text{DN}_{\text{random}}^{\text{state }k}). \tag{11}$$

Dark current and random noise errors are introduced in the calibration of the measurement matrix if the image gray level of CCD is used to replace the output Stokes vector. The number of incident photons and charges collected by each detection unit differs when photoelectric conversion of incident light radiation is conducted, and the response of each pixel is not uniform due to various noise factors. Similarly, the proportional coefficients (α and β) and noise coefficients ($\text{DN}_{\text{dark}}^{\text{state }k}$ and $\text{DN}_{\text{random}}^{\text{state }k}$) of each detection unit are not identical. However, calibrating the measurement matrix of each modulated polarization state of each detection unit requires complex calculations, a large amount of data, and increased calculation time when the

polarization state of unknown incident light is retrieved. These conditions are not beneficial for the shooting of dynamic scenes.

We minimize the condition number of DRM to select the calibration polarization state, simplify the calibration process, and reduce the operation time of the system [22]. Considering the random noise error, we adopt multiple sampling to obtain the average value and then use the least-squares method to identify the global uniform optimal solution of a measurement matrix X. The spatial non-uniformity of the four raw frames of the incident light with unknown polarization state obtained by the polarimeter modulated by the FLC cells should be corrected after the determination of the global measurement matrix X^{-1} to further correct the non-uniformity error. This process ensures the spatial consistency of $S_{0,\mathrm{out}}^{\mathrm{frame1}}$, $S_{0,\mathrm{out}}^{\mathrm{frame2}}$, $S_{0,\mathrm{out}}^{\mathrm{frame3}}$, $S_{0,\mathrm{out}}^{\mathrm{frame4}}$ of each pixel under four modulated polarization states. The spatial uniformity of the estimated Stokes vectors $S_{0,\mathrm{in}}$, $S_{1,\mathrm{in}}$, $S_{2,\mathrm{in}}$, $S_{3,\mathrm{in}}$ of incident light can be guaranteed, and the spatial uniformity of the calculated results of polarization information can likewise be ensured.

B. Method of Non-Uniformity Correction

In this section, we describe a procedure that can be used to calibrate the LCMP without knowing the details of the various errors introduced by the components that comprise the polarimeter. As discussed in the analysis in Section 3.A, the key to addressing the spatial non-uniformity of polarization is to correct the four initial frames of the incident light received by the detector after modulation by the FCLs. We assume that the radiation response of the polarimeter under each modulated polarization state is linear in the unsaturated region and stable in time [23]. Thus, the output gray of each detection unit in each initial frame can be expressed as

$$DN_{ij}^{\mathrm{frame}\,k}(L) = A_{ij}^{\mathrm{frame}\,k} L + B_{ij}^{\mathrm{frame}\,k} + C_{ij}^{\mathrm{frame}\,k} \ (k = 1, 2, 3, 4), \tag{12}$$

where (i, j) are the coordinates on the focal plane of the detector, L is the irradiance of the incident light, $DN_{ij}^{\mathrm{frame}\,k}(L)$ is the output gray of each initial frame when the incident irradiance is L, $A_{ij}^{\mathrm{frame}\,k}$ is the gain coefficient of the response characteristics of each detection unit in each initial frame, and $B_{ij}^{\mathrm{frame}\,k}$ and $C_{ij}^{\mathrm{frame}\,k}$ are offsets caused by dark current noise and random noise, respectively.

For each detection unit of each initial frame, the values of $A_{ij}^{\mathrm{frame}\,k}$ and $B_{ij}^{\mathrm{frame}\,k}$ are fixed. Thus, one of the reasons for the spatial non-uniformity of each initial frame is that the coefficients $A_{ij}^{\mathrm{frame}\,k}$ and $B_{ij}^{\mathrm{frame}\,k}$ of each detection unit in the same initial frame are different. Another reason is the existence of unstable random noise $C_{ij}^{\mathrm{frame}\,k}$. Moreover, the shot noise and reading noise in random noise obey the Gauss distribution and have the characteristic of zero mathematical expectation. Therefore, the mean of the random offset coefficient $C_{ij}^{\mathrm{frame}\,k}$ is zero. The average value of multiple sampling can be used to minimize the influence of random noise on the output gray to obtain

$$\overline{\mathrm{DN}_{ij}^{\mathrm{frame}\,k}(L)} = A_{ij}^{\mathrm{frame}\,k} L + \overline{B_{ij}^{\mathrm{frame}\,k}}, \tag{13}$$

where $\overline{\mathrm{DN}_{ij}^{\mathrm{frame}\,k}(L)}$ and $B_{ij}^{\mathrm{frame}\,k}$ denote the averages of the output gray value and dark current offset after repeated measurements, respectively.

Given the linear response of the detector, we use the following formula to correct the difference between coefficients $A_{ij}^{\mathrm{frame}\,k}$ and $B_{ij}^{\mathrm{frame}\,k}$ of each detection unit in each initial frame:

$$\mathrm{DNC}_{ij}^{\mathrm{frame}\,k}(L) = G_{ij}^{\mathrm{frame}\,k} \cdot \overline{\mathrm{DN}_{ij}^{\mathrm{frame}\,k}(L)} + O_{ij}^{\mathrm{frame}\,k}, \tag{14}$$

where $G_{ij}^{\mathrm{frame}\,k}$ and $O_{ij}^{\mathrm{frame}\,k}$ are the correction gains and offsets of the detector position (i, j), respectively, and $\mathrm{DNC}_{ij}^{\mathrm{frame}\,k}(L)$ is the corrected output gray value. $G_{ij}^{\mathrm{frame}\,k}$ and $O_{ij}^{\mathrm{frame}\,k}$ can be obtained using the output response of each detection unit on the focal plane under two different radiation intensities of a uniform light source.

The two radiation intensities are selected as a relatively small value L_s and a relatively large value L_l besides input minimum and near-saturation values. The selection of two radiation intensities directly affects the accuracy of the correction method. A calibration radiation intensity selection method based on dichotomy is applied here. It is assumed that the slope of the straight line is k_1 for connecting the selected low and medium radiation intensity points, and k_2 for the high and medium radiation intensity points. If k_1 and k_2 are equal or the difference between k_1 and k_2 is less than a threshold δ (which is usually an empirical value based on image quality), the selected low and high radiation intensity points can be considered suitable.

By introducing L_s and L_l into Eq. (14), we can obtain

$$\mathrm{DNC}_{ij}^{\mathrm{frame}\,k}(L_s) = G_{ij}^{\mathrm{frame}\,k} \cdot \overline{\mathrm{DN}_{ij}^{\mathrm{frame}\,k}(L_s)} + O_{ij}^{\mathrm{frame}\,k}, \tag{15}$$

$$\mathrm{DNC}_{ij}^{\mathrm{frame}\,k}(L_l) = G_{ij}^{\mathrm{frame}\,k} \cdot \overline{\mathrm{DN}_{ij}^{\mathrm{frame}\,k}(L_l)} + O_{ij}^{\mathrm{frame}\,k}. \tag{16}$$

M frame images are captured when the radiation intensity is L_s and L_l. The average values of these images are obtained, and the response values of each detection unit of the average image are normalized to obtain $\overline{\mathrm{DN}_1^{\mathrm{frame}\,k}}$ and $\overline{\mathrm{DN}_2^{\mathrm{frame}\,k}}$ as follows:

$$\overline{\mathrm{DN}_1^{\mathrm{frame}\,k}} = \frac{1}{I \times J} \sum_{i=1}^{I} \sum_{j=1}^{J} \overline{\mathrm{DN}_{ij}^{\mathrm{frame}\,k}(L_s)}, \tag{17}$$

$$\overline{\mathrm{DN}_2^{\mathrm{frame}\,k}} = \frac{1}{I \times J} \sum_{i=1}^{I} \sum_{j=1}^{J} \overline{\mathrm{DN}_{ij}^{\mathrm{frame}\,k}(L_l)}, \tag{18}$$

where $I \times J$ is the number of pixels in the detector. The correction gain and offset can be calculated by the following formula:

$$G_{ij}^{\mathrm{frame}\,k} = \frac{\overline{\mathrm{DN}_2^{\mathrm{frame}\,k}} - \overline{\mathrm{DN}_1^{\mathrm{frame}\,k}}}{\overline{\mathrm{DN}_{ij}^{\mathrm{frame}\,k}(L_l)} - \overline{\mathrm{DN}_{ij}^{\mathrm{frame}\,k}(L_s)}}, \tag{19}$$

$$O_{ij}^{\mathrm{frame}\,k} = \frac{\overline{\mathrm{DN}_2^{\mathrm{frame}\,k}} \times \overline{\mathrm{DN}_{ij}^{\mathrm{frame}\,k}(L_s)} - \overline{\mathrm{DN}_1^{\mathrm{frame}\,k}} \times \overline{\mathrm{DN}_{ij}^{\mathrm{frame}\,k}(L_l)}}{\overline{\mathrm{DN}_{ij}^{\mathrm{frame}\,k}(L_s)} - \overline{\mathrm{DN}_{ij}^{\mathrm{frame}\,k}(L_l)}}. \tag{20}$$

Each pixel of the polarimeter's four initial frames can have the same output response under the same irradiation conditions by multiplying the actual pixel response signal with its gain coefficients and adding offset. Accordingly, the non-uniformity correction of the four initial frames can be realized, and the non-uniformity of the Stokes vectors is further corrected as shown as follows in Eq. (21):

$$\begin{bmatrix} S^{\mathrm{cor}}_{0,ij,\mathrm{in}} \\ S^{\mathrm{cor}}_{1,ij,\mathrm{in}} \\ S^{\mathrm{cor}}_{2,ij,\mathrm{in}} \\ S^{\mathrm{cor}}_{3,ij,\mathrm{in}} \end{bmatrix} = X^{-1} \begin{bmatrix} \mathrm{DNC}^{\mathrm{frame1}}_{ij} \\ \mathrm{DNC}^{\mathrm{frame2}}_{ij} \\ \mathrm{DNC}^{\mathrm{frame3}}_{ij} \\ \mathrm{DNC}^{\mathrm{frame4}}_{ij} \end{bmatrix} = X^{-1} \begin{bmatrix} G^{\mathrm{frame1}}_{ij} \cdot \overline{\mathrm{DN}^{\mathrm{frame1}}_{ij}(L)} + O^{\mathrm{frame1}}_{ij} \\ G^{\mathrm{frame2}}_{ij} \cdot \overline{\mathrm{DN}^{\mathrm{frame2}}_{ij}(L)} + O^{\mathrm{frame2}}_{ij} \\ G^{\mathrm{frame3}}_{ij} \cdot \overline{\mathrm{DN}^{\mathrm{frame3}}_{ij}(L)} + O^{\mathrm{frame3}}_{ij} \\ G^{\mathrm{frame4}}_{ij} \cdot \overline{\mathrm{DN}^{\mathrm{frame4}}_{ij}(L)} + O^{\mathrm{frame4}}_{ij} \end{bmatrix}. \quad (21)$$

The polarization information of incident light in each detection unit of the polarimeter is calculated with the corrected Stokes vectors. The DOLP, AOP, DOCP, and EP can be computed by Eqs. (22)–(25). The uniformity of the spatial response of the polarization states is guaranteed because the spatial non-uniformity of the Stokes vectors is corrected;

$$\mathrm{DOLP}^{\mathrm{cor}}_{ij} = \frac{\sqrt{(S^{\mathrm{cor}}_{1,ij,\mathrm{in}})^2 + (S^{\mathrm{cor}}_{2,ij,\mathrm{in}})^2}}{S^{\mathrm{cor}}_{0,ij,\mathrm{in}}}, \quad (22)$$

$$\mathrm{AOP}^{\mathrm{cor}}_{ij} = \frac{1}{2}\mathrm{Arg}(S^{\mathrm{cor}}_{1,ij,\mathrm{in}} + iS^{\mathrm{cor}}_{2,ij,\mathrm{in}}), \quad (23)$$

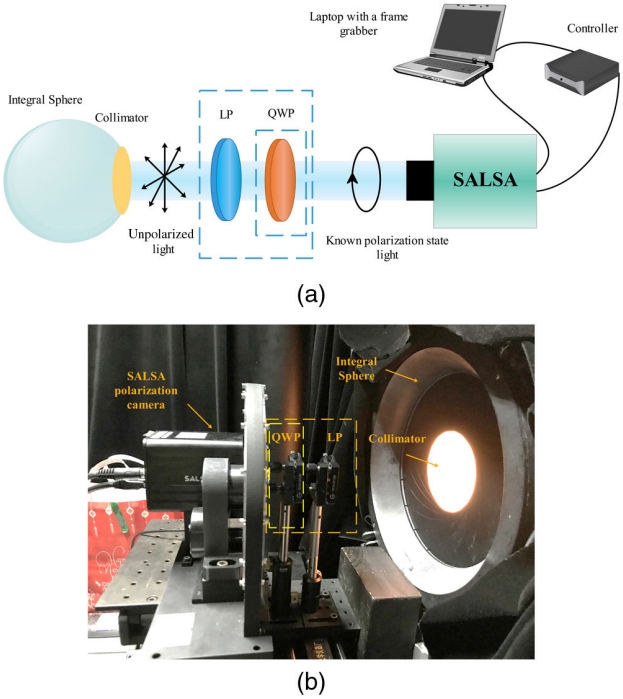

Fig. 2. Experimental equipment: (a) schematic and (b) practical calibration platform.

$$\mathrm{DOCP}^{\mathrm{cor}}_{ij} = \frac{S^{\mathrm{cor}}_{3,ij,\mathrm{in}}}{S^{\mathrm{cor}}_{0,ij,\mathrm{in}}}, \quad (24)$$

$$\mathrm{EP}^{\mathrm{cor}}_{ij} = \frac{1}{2}\mathrm{Arc\,sin}\left(\frac{S^{\mathrm{cor}}_{3,ij,\mathrm{in}}}{S^{\mathrm{cor}}_{0,ij,\mathrm{in}}}\right). \quad (25)$$

4. VALIDATION EXPERIMENTS AND EFFECTIVENESS ANALYSIS

A. Experimental Setup

The validity of the correction method is further verified by experiments. The diagram and physical drawings of the experimental configuration are shown in Fig. 2. The illumination source is an integral sphere that can emit uniform radiation light. Its uniformity error is less than ±0.5%. A collimator is used to simulate parallel light at infinity. A linear polarizer

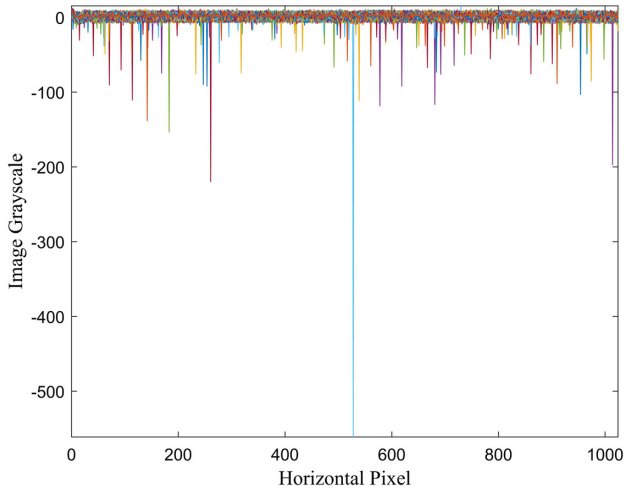

Fig. 3. Output gray response of raw frame 1.

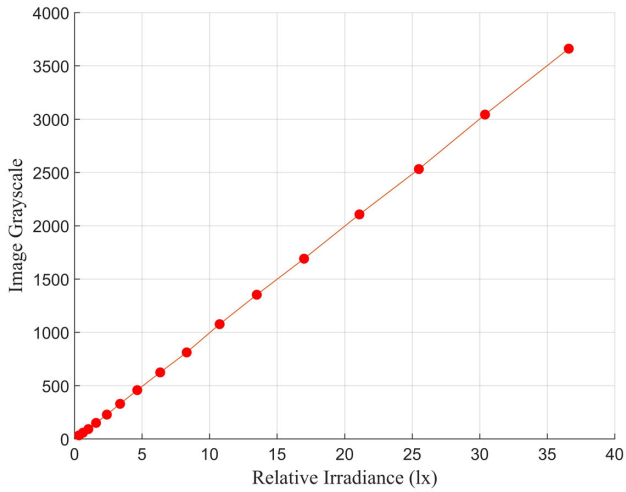

Fig. 4. Gray response of the detector under different irradiances. The red points represent the sampling points. The linear relationship between the response and radiation intensity is evident in the red fitting curve.

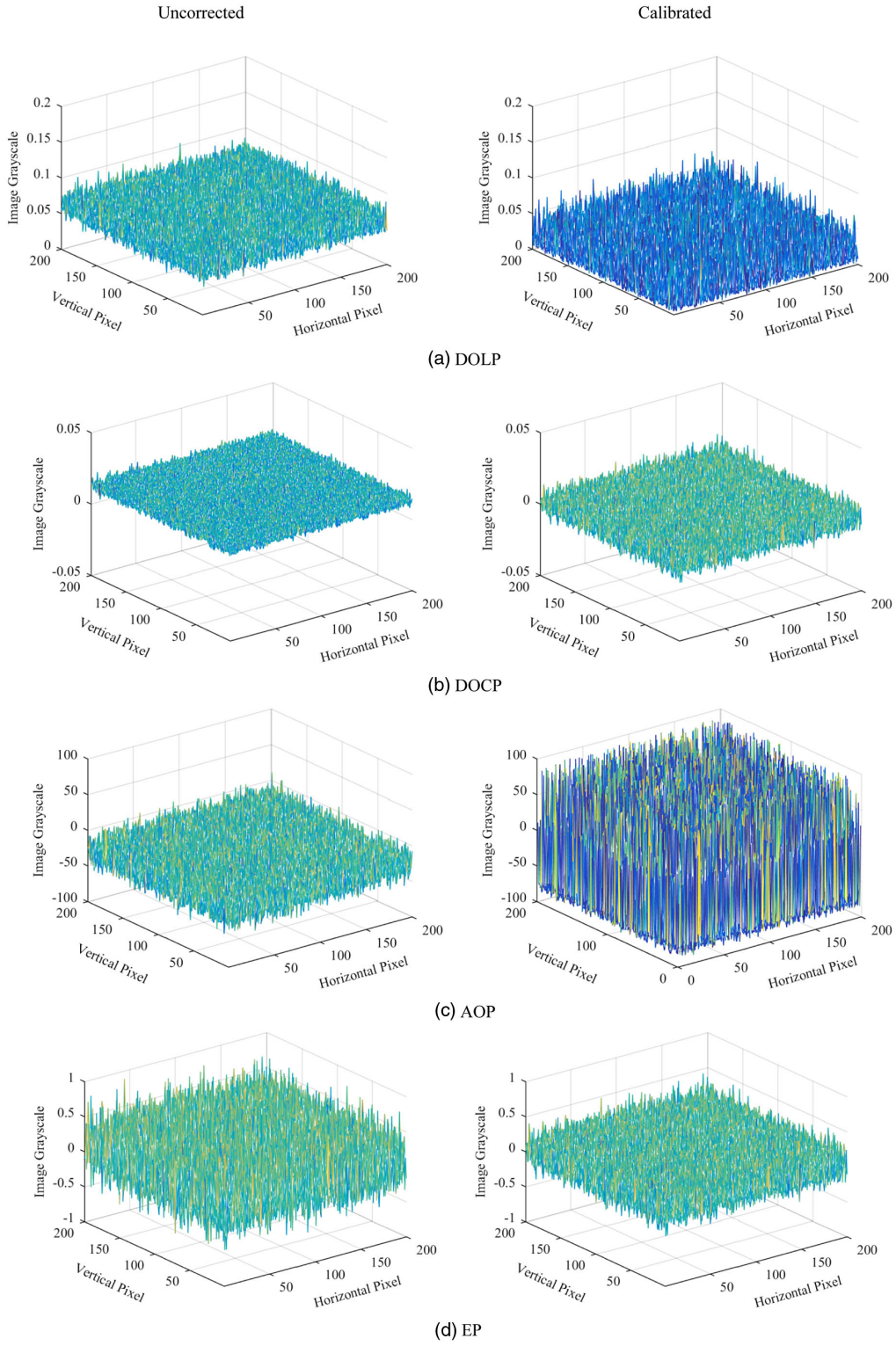

Fig. 5. Experimental result comparison: (a) DOLP, (b) AOP, (c) DOCP, and (d) EP.

(Thorlabs LPVISE100-A) with extinction ratio greater than 5000:1 and a quarter-wave plate (DHC GCL-0604, 532 nm) are employed to generate the various input Stokes vectors. A liquid crystal modulated full-Stokes polarization camera (SALSA, Bossa Nova Vision) is used to obtain the polarization states of incident light and verify the algorithm. The experimental environment is a dark room with a temperature of 22°C.

After the experimental equipment is installed, the effectiveness of the proposed correction algorithm is verified through the following steps.

First, verify the hypothesis of dark current noise and random noise. Start the polarization camera and controller. After 30 min of preheating, 20 measurements should be made without the light source, linear polarizer, and quarter-wave plate.

Second, verify the linear relationship between the radiation intensity of the incident light and the response of the detector. Adjust the voltage of the light source to change the incident intensity and collect the initial frame images.

Finally, verify the effectiveness of the correction method. After the correction coefficient is calculated using the method proposed in Section 3, the linear polarizer is placed between the light source and camera to produce the linear polarized light. The quarter-wave plate is placed between the linear polarizer and the camera, and circularly polarized light is generated by setting the fast axis of the quarter-wave plate and polarization direction of the linear polarizing plate at an angle of 45°. The polarization images are then obtained. Compare the spatial uniformity of the calculated DOLP, DOCP, AOP, and EP before and after correction.

B. Experimental Results and Analysis

1. Laboratory Calibration

The mean values of multiframe image measurements are utilized as the final experimental results to reduce the influence of random noise. The experimental results and data analysis are as follows. The output gray response of each pixel of the raw frame 1 at gain of 10 dB and exposure time of 40 ms is shown in Fig. 3. For observation, the monitor image is a 2D projection of an original 3D image. The figure shows that the response output of the detector is mostly concentrated near zero, but many dark current and blind pixel noises exist.

The abnormal noise value is defined as the measurement value whose deviation from the mean value is more than 3 times the standard deviation. After calculating the mean value and standard deviation of the gray value of the raw frame 1, the ratio of the number of pixels with abnormal noise value to all the pixels is 0.17%. The responses of the three other frames are similar to those of frame 1, so they are not listed here. These noises may cause deviation between the calculated results and the real values of the polarization state, which is one of the reasons for the non-uniformity.

The gray response of the detector under different irradiances is shown in Fig. 4. The linear equation of frame 1 fitting is

$$\overline{\mathrm{DN}^{\mathrm{frame\,1}}}(L) = 100.2L - 9.478. \tag{26}$$

The noise and gray response of the polarimeter meet the hypothesis of our proposed correction algorithm.

Here the slope threshold is set to $\delta = 2$. We select two relative radiation intensities in the unsaturated region of the CCD for non-uniformity correction, $L_s = 1.03lx$ and $L_l = 36.6lx$. The calculated slope difference is

$$|k_2 - k_1| = |100.7404 - 98.7974| = 1.9430 < 2. \tag{27}$$

Therefore, the selected calibration points are reasonable. Then the correction gain coefficient and bias coefficient can be calculated by introducing the average value of the grayscale response of all the pixels corresponding to these two points into Eqs. (19) and (20). Finally, the polarization information can be reconstructed according to the description in Section 3.B. To further prove the effectiveness of the proposed method, we compare the spatial uniformity of the polarization states measured before and after correction when the incident light is non-polarized, linearly polarized, and circularly polarized. The comparison results before and after correction of non-polarized light are shown in Fig. 5.

In Fig. 5, the first image is the 3D distribution of the polarization parameters before correction, and the second image is the corrected version. The four rows are the numerical distributions of the DOLP, AOP, DOCP, and EP. Under non-polarized light incidence, the DOLP, DOCP, and EP should be equal to 0, and the AOP should be randomly distributed in the range of −90° to +90°. A comparison of the figures shows that the polarization parameters before correction are deviated from the actual situation, and the polarization parameters after correction by the proposed method tend to be true values.

The theoretical values and the uncorrected and corrected mean and root mean square error (RMSE) of the DOLP, DOCP, AOP, and EP are compared to quantitatively illustrate the performance of this correction method. The formula of RMSE is described by Eq. (28) as follows:

Table 1. Upper Limit of RMSE

Polarization States of Incident Light	Polarization Parameters	Theoretical Value	Maximum Deviation	Upper Limit of RMSE
Non-polarized light	DOLP	0	1	1
	DOCP	0	1	1
	EP (°)	0	45	45
Linearly polarized light	DOLP	1	0	1
	DOCP	0	1	1
	AOP (°)	90	−90	180
	EP(°)	0	45	45
Circularly polarized light	DOLP	0	1	1
	DOCP	1	0	1
	EP (°)	45	−45	−90

Table 2. Non-Polarized Light

Polarization Parameters	Theoretical Value	Uncorrected Mean	Corrected Mean	Uncorrected RMSE	Corrected RMSE
DOLP	0	0.0620	**0.0198**	0.0627	**0.0240**
DOCP	0	0.0131	**0.0015**	0.0133	**0.0047**
EP (°)	0	0.0877	**0.0425**	0.2270	**0.1343**

Table 3. Linearly Polarized Light

Polarization Parameters	Theoretical Value	Uncorrected Mean	Corrected Mean	Uncorrected RMSE	Corrected RMSE
DOLP	1	0.9868	**0.9934**	0.0382	**0.0362**
DOCP	0	0.0304	**0.0022**	0.0314	**0.0223**
AOP (°)	70	68.3599	**70.8833**	3.6513	**3.5992**
EP (°)	0	−0.1131	**−0.0634**	1.2576	**0.6389**

Table 4. Circularly Polarized Light

Polarization Parameters	Theoretical Value	Uncorrected Mean	Corrected Mean	Uncorrected RMSE	Corrected RMSE
DOLP	0	0.2664	**0.0757**	0.2698	**0.0924**
DOCP	1	1.4397	**1.2741**	0.0227	**0.0183**
EP (°)	45	47.7669	**45**	2.8067	**0**

Table 5. RMSE Results Comparison of the Computer Monitor

Polarization Parameters	Uncorrected RMSE	Corrected RMSE	RMSE Reduction Rate
DOLP	0.4899	**0.4879**	0.41%
DOCP	0.6677	**0.6635**	0.63%
AOP (°)	6.8917	**4.1265**	40.12%
EP (°)	3.3075	**2.1070**	36.30%

$$\mathrm{RMSE}_p = \sqrt{\frac{1}{I \times J}\sum_{i=1}^{I}\sum_{j=1}^{J}[V_p(i,j) - T(p)]^2}. \quad (28)$$

Here $V_p(i, j)$ represents the measured and corrected values of each detection unit (i, j) of the DOLP, DOCP, AOP, and EP. $T(p)$ represents the theoretical value of each polarization parameter. The optimal solution of the RMSE is zero, which means that the measured value is consistent with the theoretical value, and the error is zero. The smaller the RMSE value, the smaller the error. Table 1 lists the theoretical values of each polarization parameter when the incident light is in different polarization states; the measured readings are at the maximum theoretical deviation and the upper limit of the RMSE for better understanding of how much the RMSE has been reduced with the correction method.

The calculated results of the polarization parameters of incident light with different polarization states are compared in Tables 2–4. The boldfaced numbers in the tables represent the corrected mean and RMSE values. No comparison is made in Tables 2 and 4 because the AOP is randomly distributed in the range of −90° to +90° when the incident light is non-polarized and uniformly circularly polarized.

As shown in Table 2, when the non-polarized light is incident, the polarization parameters are corrected and then return to the vicinity of the value of 0. Moreover, the effects of dark current and random noises are weakened. The data in Table 2 show that the corrected mean value of each polarization parameter is close to the theoretical value when the uniform linearly polarized light is incident. Furthermore, the RMSE of DOLP is decreased by 5.08%, and the RMSE of AOP is decreased by 1.43%. Similarly, Table 3 indicates that the mean values of the corrected DOCP and EP are close to the theoretical values. The RMSE of the DOCP decreases by as much as 19%, and the RMSE of the EP becomes nearly zero after correction.

The proposed correction algorithm may not be particularly effective for a single raw frame, but the polarization parameters calculated from the four corrected raw frames are well corrected. The proposed correction algorithm is effective and operable and can reduce measurement errors.

2. Real Scene

In order to prove the validity of this correction algorithm in a real scene, we take a computer monitor as the observation object and collect the intensity and polarization images before and after correction. For observing the correction effect more conveniently, we processed the image with proper pseudo-color processing. The comparison results are shown in Fig. 6. The third row presents the enlarged contrast before and after the correction of the red box areas. It can be seen that the intensity

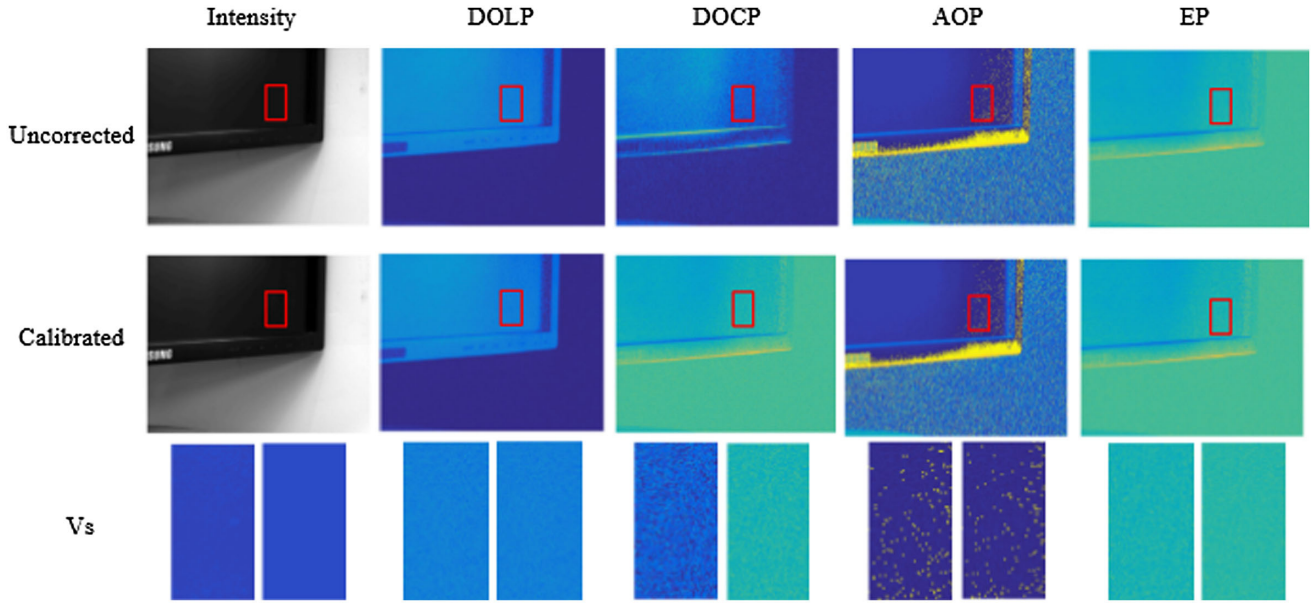

Fig. 6. Overcorrection comparison of intensity and polarization images.

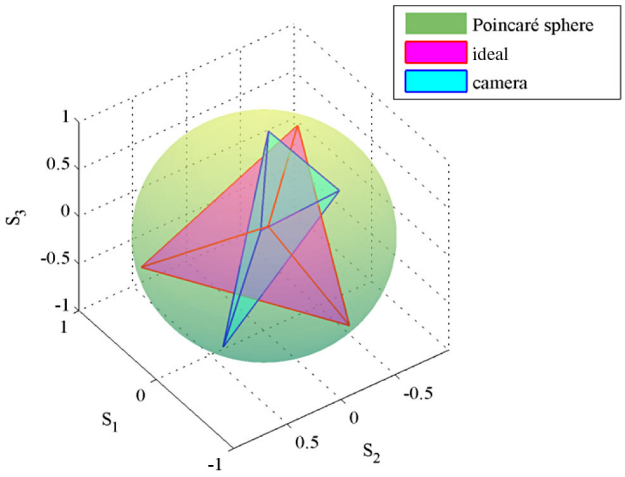

Fig. 7. Position of the ideal tetrahedron and the tetrahedron constructed by the eigenstates of the polarization analyzer used in the camera on the Poincaré sphere.

and polarization images of the same object after correction are more uniform and less noisy.

We also calculated the RMSE of the polarization parameters before and after correction. The comparison results are shown in Table 5. Thus, the correction effect of this algorithm on AOP and EP is more obvious. In addition, it is worth mentioning that the calibration process may consume a certain amount of time, but after calibration, the gain coefficient and bias coefficient of each pixel can be stored in advance, and the response value of the detector can be continuously corrected in the detection process. Four polarization images of 1024×1024 pixels can be reconstructed in about 14 s.

However, it can be seen that the residual noise still exists in the reconstructed polarization information. The reason may be related to the position of the sampling point of the camera. Figure 7 shows the position of the ideal tetrahedron and the tetrahedron constructed by the eigenstates of the polarization analyzer used in the camera on the Poincaré sphere. The measurement matrix X is extracted to form four vertex coordinates besides the first column, and the four vertices are connected to form a closed blue tetrahedron in Fig. 7. The volumes of the two tetrahedrons are calculated to be $V_{\text{camera}} = 0.1450$ and $V_{\text{ideal}} = 0.5132$, respectively. This means that the measurement result of the Stokes vector of the polarization analyzer is more susceptible to noise, and its error sensitivity is relatively high. Therefore, more stable sampling methods in future research should be attempted to further reduce the error.

5. CONCLUSION

In this paper, a method of correcting the spatial response non-uniformity of polarization states on the basis of the premise of linear detector response for LCMPs is presented. Starting with the analysis of many factors causing non-uniformity, such as dark current noise, random noise, and fabrication defects, a theoretical model of Stokes vectors with non-uniformity noise is established. The response output is corrected by obtaining the mean value and calculating the correction gain coefficient and bias coefficient. Consequently, the spatial output value of each polarization parameter tends to be the same under the same uniformly polarized incident light. The advantages of the proposed method over sub-area calibration and sub-component calibration are simplicity of calibration and low computational complexity. For LCMPs with a calibrated Mueller matrix, the components do not need to be separated for error analysis, and the transmission matrix does not require recalibration. The experimental results show that the proposed algorithm is effective for LCMP cameras and performs well in improving the measurement accuracy of polarization parameters. In addition, this method can be employed in other polarization detection systems with linear response to improve precision.

Funding. National Natural Science Foundation of China (NSFC) (61705225).

REFERENCES

1. J. S. Tyo, D. L. Goldstein, D. B. Chenault, and J. A. Shaw, "Review of passive imaging polarimetry for remote sensing applications," Appl. Opt. **45**, 5453–5469 (2006).
2. F. Liu, L. Cao, X. Shao, P. Han, and X. Bin, "Polarimetric dehazing utilizing spatial frequency segregation of images," Appl. Opt. **54**, 8116–8122 (2015).
3. Y. Ding and S. Pau, "Circularly and elliptically polarized light under water and the Umov effect," Light Sci. Appl. **8**, 32 (2019).
4. W. de Jong, "Infrared polarization measurements and modeling applied to surface-laid antipersonnel landmines," Opt. Eng. **41**, 1021 (2002).
5. E. Compain and B. Drevillon, "Broadband division-of-amplitude polarimeter based on uncoated prisms," Appl. Opt. **37**, 5938–5944 (1998).
6. J. A. Shaw, J. L. Pezzaniti, J. S. Tyo, and D. B. Chenault, "A division of aperture MWIR imaging polarimeter," Proc. SPIE **5888**, 58880V (2005).
7. G. Myhre, W.-L. Hsu, A. Peinado, C. LaCasse, N. Brock, R. A. Chipman, and S. Pau, "Liquid crystal polymer full-Stokes division of focal plane polarimeter," Opt. Express **20**, 27393–27409 (2012).
8. M. W. Kudenov, M. J. Escuti, E. L. Dereniak, and K. Oka, "White-light channeled imaging polarimeter using broadband polarization gratings," Appl. Opt. **50**, 2283–2293 (2011).
9. Y. Huang, Z. He, and S.-T. Wu, "Fast-response liquid crystal phase modulators for augmented reality displays," Opt. Express **25**, 32757–32766 (2017).
10. Z. He, Y.-H. Lee, F. Gou, D. Franklin, D. Chanda, and S.-T. Wu, "Polarization-independent phase modulators enabled by two-photon polymerization," Opt. Express **25**, 33688–33694 (2017).
11. Z. He, G. Tan, D. Chanda, and S.-T. Wu, "Novel liquid crystal photonic devices enabled by two-photon polymerization [Invited]," Opt. Express **27**, 11472–11491 (2019).
12. M. Vedel, S. Breugnot, and N. Lechocinski, "Full Stokes polarization imaging camera," Proc. SPIE **8160**, 81600X (2011).
13. J. Chu, W. Lin, R. Zhang, and Y. Chen, "Image registration of polarimeters," Opt. Precis. Eng. **26**, 1181–1190 (2018).
14. D. Zhao, T. Lenz, G. H. Gelinck, P. Groen, D. Damjanovic, D. M. de Leeuw, and I. Katsouras, "Depolarization of multidomain ferroelectric materials," Nat. Commun. **10**, 2547 (2019).
15. J. C. Gladish and D. D. Duncan, "Alignment and temperature effects in liquid-crystal-based active polarimetry," Appl. Opt. **53**, 3982–3992 (2014).
16. E. Compain, S. Poirier, and B. Drevillon, "General and self-consistent method for the calibration of polarization modulators, polarimeters, and Mueller-matrix ellipsometers," Appl. Opt. **38**, 3490–3502 (1999).
17. M. Vedel, S. Breugnot, and N. Lechocinski, "Spatial calibration of full Stokes polarization imaging camera," Proc. SPIE **9099**, 90990I (2014).

18. H. Zhang, Y. Li, C. Yan, and J. Zhang, "Calibration of polarized effect for time-divided polarization spectral measurement system," Opt. Precis. Eng. **25**, 325–333 (2017).
19. G. G. Stokes, "On the composition and resolution of streams of polarized light from different sources," Trans. Cambridge Philos. Soc. **9**, 399 (1852).
20. R. A. Chipman, "Polarimetry," in *Handbook of Optics* (McGraw-Hill, 1995), Vol. **2**, Chap. 22.
21. R. Widenhorn, I. Hartwig, J. C. Dunlap, and E. Bodegom, "Influence of illumination on dark current in charge-coupled device imagers," J. Electron. Imaging **18**, 033015 (2009).
22. Y. Quéau, F. Leporcq, and A. Alfalou, "Design and simplified calibration of a Mueller imaging polarimeter for material classification," Opt. Lett. **43**, 4941–4944 (2018).
23. H. Zhou, S. Liu, R. Lai, D. Wang, and Y. Cheng, "Solution for the nonuniformity correction of infrared focal plane arrays," Appl. Opt. **44**, 2928–2932 (2005).